Published in final edited form as:

Nat Chem. 2020 March ; 12(3): 276–283. doi:10.1038/s41557-019-0409-4.

Nickel-catalysed anti-Markovnikov hydroarylation of unactivated alkenes with unactivated arenes facilitated by non-covalent interactions

Noam I. Saper[1], **Akito Ohgi**[2], **David W. Small**[1], **Kazuhiko Semba**[2], **Yoshiaki Nakao**[2,*], **John F. Hartwig**[1,*]

[1]Department of Chemistry, University of California, Berkeley, Berkeley, CA, USA.

[2]Department of Material Chemistry, Graduate School of Engineering, Kyoto University, Kyoto, Japan.

Abstract

Anti-Markovnikov additions to alkenes have been a longstanding goal of catalysis, and anti-Markovnikov addition of arenes to alkenes would produce alkylarenes that are distinct from those formed by acid-catalysed processes. Existing hydroarylations are either directed or occur with low reactivity and low regioselectivity for the *n*-alkylarene. Herein, we report the first undirected hydroarylation of unactivated alkenes with unactivated arenes that occurs with high regioselectivity for the anti-Markovnikov product. The reaction occurs with a nickel catalyst ligated by a highly sterically hindered N-heterocyclic carbene. Catalytically relevant arene- and alkene-bound nickel complexes have been characterized, and the rate-limiting step was shown to be reductive elimination to form the C–C bond. Density functional theory calculations, combined with second-generation absolutely localized molecular orbital energy decomposition analysis, suggest that the difference in activity between catalysts containing large and small carbenes results more from stabilizing intramolecular non-covalent interactions in the secondary coordination sphere than from steric hindrance.

Linear alkylbenzenes are fundamental precursors to a variety of industrially relevant surfactants, detergents, plastics and fine chemicals[1] with a global market value of over US$7.75 billion (ref.[2]). Although termed ‘linear alkylbenzenes’, the commercial process for their formation leads to mixtures of isomeric branched alkylbenzenes from the

[*]**Correspondence and requests for materials** should be addressed to Y.N. or J.F.H. nakao.yoshiaki.8n@kyoto-u.ac.jp; jhartwig@berkeley.edu.

Author contributions

All authors conceived and designed the experiments. N.I.S., A.O. and K.S. performed the experiments. N.I.S. and D.W.S. performed the computations. All authors participated in discussion and N.I.S. J.F.H. and Y.N. co-wrote the manuscript.

Online content

Any Nature Research reporting summaries, source data, extended data, supplementary information, acknowledgements, peer review information; details of author contributions and competing interests; and statements of data and code availability are available at https://doi.org/10.1038/s41557-019-0409-4.

Competing interests

The authors declare no competing interests

Supplementary information is available for this paper at https://doi.org/10.1038/s41557-019-0409-4.

rearrangement of carbocationic intermediates in the alkylation step[3]. Because branched alkylarenes are more resistant to biodegradation[4], their use as surfactants and detergents has led to the extensive pollution of rivers, lakes and oceans[5,6].

Anti-Markovnikov transition-metal catalysed hydroarylation could lead to *n*-alkylbenzenes, but the reaction of unactivated alkenes with simple unactivated arenes lacking a directing group[7–10] has not been reported with high selectivity for the linear product (Fig. 1a). The iridium, ruthenium and platinum systems reported by Periana[11–15], Gunnoe[16–18] and Goldberg[19,20] and their co-workers all catalyse the reaction of benzene (**1**) with propylene (**2**) to provide alkylarenes **3** and **4** with moderate activity, but give nearly 1:1 ratios of the constitutional isomers (Fig. 1b). Gunnoe and co-workers recently reported a two-step synthesis of *n*-alkylarenes by rhodiumcatalysed oxidative alkenylation and hydrogenation, but the process involves two steps and a copper salt as the co-catalyst[21,22].

The regioselectivity of published undirected hydroarylations is controlled by the regioselectivity of insertion of the alkene into the metal–aryl bond (1,2 vs 2,1 addition)[13,17,23–25]. By this mechanism, high selectivity for the linear product requires that insertion form a branched alkylmetal intermediate, but such an intermediate is typically less stable than the linear alkylmetal isomer. Moreover, the rates of these processes are likely limited by the counterbalancing electronic effects on the oxidative addition of an aryl C–H bond, which is often faster to more electron-rich metal centres than electron-poor metal centres[24,26–31], and migratory insertion, which is often faster into metal–ligand bonds of more electron-poor metal centres than of more electron-rich metal centres[32].

A catalytic cycle that operates by an alternative mechanism could enable higher levels of regioselectivity for the linear product and bypass the counterbalancing electronic effects on multiple steps. Previous research by our groups led to a nickel-catalysed, linear-selective hydroarylation with electron-deficient arenes[33] and various electronically activated heteroarenes[34], but the reactions of electron-neutral arenes, such as benzene or alkylarenes, occurred with low turnovers. Thus, an analysis of the factors controlling activity was needed to achieve the first addition of an unactivated arene to a terminal alkene in good yield with high linear selectivity. In the most favourable case, this reaction would occur with a catalyst based on an earth-abundant, non-precious metal.

We report here undirected hydroarylations of electron-neutral arenes with unconjugated terminal alkenes that occur in good yields with exceptionally high linear/branched selectivity (>50:1 in most cases, Fig. 1c) catalysed by a nickel complex containing an outsized N-heterocyclic carbene (NHC). The reaction occurs via the formation of an alkylnickel–aryl intermediate by an unusual ligand-to-ligand hydrogen transfer (LLHT) to the coordinated alkene[33,35] and rate-determining reductive elimination. The results of computational studies imply that the attractive interactions of the large NHC ligand, rather than steric hindrance, lead to the high activity of the nickel–carbene complex.

Results and discussion

Reaction development.

Initial studies[33] showed that the combination of [Ni(COD)$_2$] (COD, cycloocta-1,5-diene) and the common NHC ligand IPr (**L1**; see Fig. 2a) led to the addition of benzene (**1**) to 1-decene (**5**) with a high linear/branched ratio of 19:1, but with a turnover of less than one. To increase the TONs, we evaluated the hydroarylation of 1-decene (**5**) with benzene (**1**) catalysed by [**L**–Ni(η^6-C_6H_6)] complexes as catalyst precursors (Fig. 2a)[36]. The yields were more reproducible, particularly at low catalyst loadings (vide infra), when catalytic amounts of NaH and Na(acac) were added. Although the reaction catalysed by [**L1**–Ni(η^6-C_6H_6)] provided only trace amounts of hydroarylation product **6**, the reactions catalysed by the complex of the more sterically encumbered ligand IPr* (**L2**)[37] and its more σ-donating analogue IPr*^{OMe} (**L3**) occurred with several turnovers[38]. Further altering the substitution of the aromatic rings on the sidearms of the NHC with 3,5-dimethylphenyl groups (**L4**, $^{m\text{-}Xyl}$IPr*^{OMe})[39] or with 3,5-diethylphenyl groups (**L5**, ^{Dep}IPr*^{OMe}) led to catalysts that gave much higher yields of the hydroarylation product (56% for **L4** and 54% for **L5** after 24 h). Alkene isomerization during the reaction by an independent process[33] decreased the concentration of the terminal alkene and reaction rates over time (Supplementary Figs. 4 and 5), but the catalysts were stable and 75 and 84% isolated yields of **6** were obtained, respectively, with **L4** or **L5** as ligand after 5 days (Table 1). The linear/branched selectivity when using **L4** or **L5** was unprecedently high at >50:1 (see above, Fig. 2a). To directly compare the relative rates of catalysts containing different NHC ligands, we measured the initial rates of the hydroarylation reaction catalysed by [**L**–Ni(η^6-C_6H_6)] (Supplementary Fig. 17). The initial rate of hydroarylation with **L4** as ligand was found to be 23 times greater than the initial rate of hydroarylation with **L1** as ligand and two times greater than the initial rate of hydroarylation with **L3** as ligand.

Benzene underwent addition to a series of unactivated alkenes (Table 1) to give the product with a linear/branched selectivity >50:1 or with undetectable amounts of branched isomer in all cases. Because [**L4**–Ni(η^6-C_6H_6)] and [**L5**–Ni(η^6-C_6H_6)] catalyse in parallel the isomerization of alkenes, the reaction of benzene (**1**) with internal alkenes, such as *trans*-4-octene (**7**), also occurred to form the n-alkylarene products in good yields. Consistent with this observation, a mixture of *cis*- and *trans*-2-hexene (**8**) and *cis*- and *trans*-3-hexene (**9**) reacted to give the n-alkylarene product in 98% yield. Terminal alkenes bearing substituents at the α-position that inhibit or prevent isomerization reacted to full conversion within 24 h. For example, alkene **10** bearing a tertiary carbon at the α-position and alkene **11** bearing a quaternary carbon at the α-position reacted to give the resulting alkylarene products in >90% yield. Both protected primary alcohols (**12**) and vinyl siloxanes (**13**) were tolerated under the reaction conditions.

The reaction of *tert*-butylethylene (**14**) with benzene occurred in nearly quantitative yield after only 1 h under the standard conditions (Table 1, entry 1). The reaction with 3 mol% catalyst without added NaH and Na(acac) provided the product in nearly the same yield as that obtained with added NaH and Na(acac) (Table 1, entry 2). However, the basic additives increased the turnover numbers of reactions conducted with low catalyst loadings. With

basic additives, the reaction with only 0.3 mol% catalyst formed the addition product in 85% yield (TON = 283, Table 1, entry 3), but without these additives, the reaction with 0.3 mol% catalyst formed the alkylarene in only 6% yield (Table 1, entry 4; for further details, see the Supplementary Information). The basic additives likely remove trace water, which affects reactions with low loadings.

The hydroarylation of unactivated alkenes also occurred with a variety of electron-neutral, electron-rich and electron-deficient arenes (Table 1). The reaction of alkene **14** with toluene provided *n*-alkylarene **15** in good yield as a mixture of *m*- and *p*-alkylarene isomers. Alkene **11** reacted with xylene isomers at the most sterically accessible position to give products **16** and **17** in moderate yields. Reactions with more electron-deficient fluoroarenes also proceeded in high yields (**18**–**21**). Finally, the intramolecular reaction of arene **22** containing a pendant alkene provided tetrahydronaphthalene **23** in 86% yield (by ^{1}H NMR spectroscopy); no cyclized product from the potential intramolecular reaction to form a five-membered ring was observed.

Investigation of the reaction mechanism.

Having developed a method for the hydroarylation reaction between unactivated arenes and alkenes that occurs in good yields with high anti-Markovnikov regioselectivity, we sought to understand the origins of the high activity of the catalysts containing ligands **L4** and **L5**. To do so, we determined experimentally the resting state of the catalyst with unhindered and hindered alkenes and the rate-determining step of the reaction, and we used a computational energy decomposition analysis[40] to identify the intramolecular interactions leading to the high activity stemming from the large ligands.

Arene-bound NHC-ligated nickel complexes were prepared on the gram scale by the addition of the free carbene ligand to a Ni^0 source in C_6H_6 as solvent under H_2 pressure[36,41]. The solid-state structures of these complexes (Fig. 2b for [**L4**–Ni(η^6-C_6H_6)]) illustrate the steric impact of the NHC ligand. In contrast to the symmetrical coordination of benzene in [**L2**–Ni(η^6-C_6H_6)], the angle between the carbene carbon and the benzene ligand in [**L4**–Ni(η^6-C_6H_6)] is significantly distorted from linearity (169.4°). This difference suggests that steric hindrance of the NHC ligand prevents a complete η^6-interaction.

To quantify the steric properties of **L4** further, the percent buried volume (% V_{Bur})[42,43] and steric map of **L4** were calculated (Fig. 2b)[44]. With the standard parameters of Dorta et al.[45] for the radius (*r*) of the sphere surrounding the metal centre of 3.5 Å, the proximal % V_{Bur} of **L4** was smaller than that of **L1** by 3%. However, with a radius of 5.5 Å to account for the remote steric environment of **L4**, the % V_{Bur} of **L4** was greater than that of **L1** by >10%. This difference is slightly greater than the difference between IPr and its *N*-(2,4,6-trimethylphenyl) analogue, known as IMes (8% difference in buried volume within 3.5 Å for L–AuCl)[42], and correlates with the large difference in activity between the catalyst containing **L1** and that containing **L4** in the hydroarylation reaction. However, the large size of **L4** cannot be solely responsible for the high reactivity of the catalyst containing **L4** in alkene hydroarylation because the reactivities of complexes of **L2** and **L3** possessing similar

steric properties (see the Supplementary Information for all % V_{Bur} values) are closer to that of the catalyst containing **L1** than to that containing **L4**.

Monitoring the reaction catalysed by the complex containing **L4** with a ^{13}C-labelled carbene carbon (**^{13C}L4**) by NMR spectroscopy revealed the resting states of the hydroarylation reactions with alkenes of varying sizes. The ^{13}C NMR spectrum of the hydroarylation reaction between **1**-d_6 and the long-chain alkene **5** recorded at 100 °C contains a resonance at 204.7 ppm (Fig. 3a), matching that of bis-alkene complex **24** generated independently in solution by combining 2.2 equiv. of alkene **5** with [**$_{13C}$L4**–Ni(η^6-C_6H_6)] (Supplementary Figs. 7 and 8). The bis-propylene analogue **25** was isolated in 50% yield from the reaction of [**L4**–Ni(η^6-C_6H_6)] and propylene (**2**; Fig. 3b) and fully characterized by NMR spectroscopy and single-crystal X-ray diffraction. The ^{13}C NMR spectrum of the reaction of the more hindered *tert*-butylethylene (**14**) obtained at 25 °C contains a single resonance at 198.7 ppm (Supplementary Fig. 11) and the colour of the solution was yellow, matching the spectrum and colour of the alkene complex **26** generated in situ from [**^{13C}L4**–Ni(η^6-C_6H_6)] and **14** (vide infra). However, the ^{13}C NMR spectrum recorded at 100 °C contains a resonance at 196.2 ppm, and the colour of the solution was red, matching those of [**^{13C}L4**–Ni(η^6-C_6D_6)]. Studies of the relative stabilities of the alkene and arene complexes by varying the amount of **14** in pentane under nitrogen (Fig. 3c,d) showed that both [**L4**–Ni(η^6-C_6H_6)] and the alkene complex **26** were present at equilibrium at lower concentrations (0.007–0.2 M) of alkene, but the mono-alkene dinitrogen complex **26**, which was identified by NMR and IR spectroscopy and single-crystal X-ray diffraction (Fig. 3e), was the only species observed at higher concentrations of alkene (0.3–0.5 M). Thus, the catalytically active species in the reactions of unhindered alkenes (such as **5**) are bis-alkene complexes, whereas those in the reactions of hindered alkenes (such as **14**) at elevated temperatures are an equilibrium mixture of mono-alkene and arene complexes.

To identify the steps of the catalytic cycle, the initial rates of the hydroarylation of both unhindered alkene **5** and hindered alkene **11** with benzene (**1**) were measured at varying alkene concentrations (Fig. 4a). The initial rate of the hydroarylation reaction with terminal alkene **5** was inverse first order in the concentration of **5** (Fig. 4a, top), indicating that one equivalent of the unhindered alkene **5** dissociates from the bis-alkene resting state **24** prior to the binding of the arene and the rate-determining step of the reaction. The order in hindered alkene **11** depended on the concentration of **11** (Fig. 4a, bottom), which is consistent with the existence of an equilibrium between the catalytic resting states as a function of the nature and concentration of the alkene, as described above (see Fig. 3d)[17,46]. The first-order dependence of the reaction rate on [**11**] at low [**11**] indicates that replacement of the arene with one alkene precedes the rate-determining step of the catalytic process, whereas the zero-order dependence of the reaction rate on [**11**] at high [**11**] indicates that the resting state shifts to the mono-alkene complex **26** and that the highest-energy transition state contains an aryl or arene unit.

Two sets of experiments revealed reversible steps within the catalytic cycle. First, the reaction of **1**-d_6 with alkene **11** led to 43% incorporation of deuterium at the 2-alkenyl position in unreacted **11** after 60% conversion (Fig. 4b). No deuterium incorporation into

the terminal position of the alkene was observed. Second, the kinetic isotope effect (KIE) determined from separate reactions of alkene **11** with either **1** or **1**-d_6 was only 1.3 ± 0.1 (Fig. 4c)[14,47]. This KIE value contrasts with the measured KIE values of 2.1–2.5 for irreversible C–H activation during ruthenium-catalysed alkene hydroarylation[17,27,28,31]. The results of both experiments imply that the transfer of the arene hydrogen to the alkene by one or multiple steps is reversible. An overall catalytic cycle for the hydroarylation of unactivated alkenes consistent with our experimental results and previous reports[33] is shown in Fig. 5a.

Computational studies using density functional theory (DFT) provided further insight into the mechanism of C−H bond cleavage (Fig. 5b, see the Supplementary Information for computational details). C−H activation could occur by oxidative addition of the C−H bond in benzene or by an alternative mechanism involving the direct transfer of the C–H bond of a coordinated arene to the bound alkene, known as ligand-to-ligand hydrogen transfer (LLHT)[35]. Previous computational studies on the nickel-catalysed hydroarylation of alkynes, hydroarylation with more acidic arenes, and hydroarylation with less hindered ligands indicated that the barrier to direct oxidative addition of the C−H bonds in benzene and other arenes to NHC-ligated Ni^0 complexes is higher than that of a one-step transfer of the hydrogen from a coordinated arene to the coordinated **π**-system of the alkene or alkyne[39,48]. The barrier we computed for the LLHT process between benzene (**1**) and propene (**2**) ligands with the catalyst containing **L4** (^{L4}**TS**$_{LLHT}$, 21.3 kcal mol^{-1}), relative to the combination of benzene and the bis-alkene ground state (**GS**), was 5.2 kcal mol^{-1} lower in energy than that for the LLHT process with the catalyst containing the less hindered **L1** (^{L1}**TS**$_{LLHT}$, 26.5 kcal mol^{-1}) and 3 kcal mol^{-1} lower than the barrier for oxidative addition of the aryl C–H bond (see the Supplementary Information for further details).

However, the highest-energy transition state of the catalytic process deduced from experiment (vide supra) and computation is the reductive elimination to form the alkyl–aryl C−C bond from T-shaped **27**, not the LLHT. The computed barrier (relative to the ground state) for reductive elimination from the alkyl aryl complex bound by **L4** (^{L4}**TS**$_{RE}$) is 29.2 kcal mol^{-1}, which is 3.9 kcal mol^{-1} lower than the computed barrier for the reductive elimination from the alkyl aryl complex bound by **L1** (^{L1}**TS**$_{RE}$). This difference is consistent with the much higher activity of [**L4**–Ni(η^6-C_6H_6)] as catalyst for the hydroarylation reaction compared with [**L1**–Ni(η^6-C_6H_6)].

One might envision this difference in barriers to result from a steric effect on the rate of reductive elimination. However, computation of the geometry and non-covalent interactions provided a much different picture of the origin of the high activity of the complex of **L4** compared with that of the smaller **L1**. Most striking, the geometrical parameters around the nickel atom in ^{L4}**TS**$_{RE}$ were found to be almost identical to those in ^{L1}**TS**$_{RE}$ (Fig. 5c), suggesting that an effect beyond simple steric effects within the transition state controls the rate.

To decipher the origin of the different barriers for reductive elimination from the complexes containing **L1** and **L4**, we used the distortion/interaction or activation strain model pioneered by Houk and co-workers[49] and the second-generation absolutely localized

molecular orbital energy decomposition analysis (ALMO-EDA) developed by Head-Gordon and co-workers[40]. Selected energy values from this analysis for the complexes of the four ligands **L1**−**L4** are summarized in Fig. 5d. A comparison of the difference in distortion energies between pairs of complexes shows that the peripheral methyl groups in **L4** ($\Delta\Delta\Delta E_{\text{dist,L4-L3}}$ = −1.5 kcal mol^{-1}), in addition to the aromatic rings ($\Delta\Delta\Delta E_{\text{dist,L2-L1}}$ = −1.1 kcal mol^{-1}), lead to distortion energies that favour reaction with **L4** over reaction with the other ligands ($\Delta\Delta\Delta E_{\text{dist,L4-L1}}$ = −2.4 kcal mol^{-1}). For all of the four NHC ligands, the NHC fragment is less distorted from the free carbene in the transition state for reductive elimination than it is in the ground state. However, this difference between the distortion energy of the carbene in the transition and ground states is greatest for **L4** and contributes to a lower barrier for the reaction of the complex containing **L4** than for the reactions of the complexes containing **L1**−**L3** (Supplementary Table 6).

This energy decomposition analysis also shows that the aryl groups in ligands **L2**−**L4**, which are not present in **L1**, lead to interaction energies that cause the barriers for reactions catalysed by complexes of **L4** (and **L2** and **L3**) to be lower than those catalysed by the complex bearing the more common ligand **L1** ($\Delta\Delta\Delta E_{\text{int,L4-L1}}$ = −4.3 kcal mol^{-1}). An analysis of the major contributions to the difference between the interaction energies in the transition state for reductive elimination with one ligand and those in the transition state for reductive elimination with another ligand can be seen in Fig. 5d. The largest differences between these values for **L4** compared with **L1** are the Pauli repulsive (steric effects), electrostatic and London dispersion terms. Assessment of each pairwise difference in these contributions to the interaction energies for the reactions catalysed by the complexes of the series of ligands reveals the structural elements of the ligands that lead to these values. This analysis shows that the Pauli repulsion term strongly influences the barrier and results principally from the larger steric impact of **L4**. Particularly striking is that this Pauli term increases the barrier for the reaction with the large ligand relative to that for the reaction with the smaller ligand, rather than decreasing the barrier ($\Delta\Delta\Delta E_{\text{Pauli,L4-L1}}$ = 5.2 kcal mol^{-1}). Typically, one presumes that steric effects cause reductive elimination involving the coupling of two ligands at a single metal centre to be faster for complexes bearing more hindered ancillary ligands[50].

In contrast, attractive electrostatic and London dispersion terms reduce the energy of the transition state containing **L4** compared with the ground state more than they reduce this difference in energy for the complexes containing the other ligands. More specifically, the values in Fig. 5d show that that presence of the eight aryl groups in ligands **L2**−**L4** lead to electrostatic interactions that are approximately 4 kcal mol^{-1} larger than the electrostatic interactions in the complexes of **L1** ($\Delta\Delta\Delta E_{\text{elstat,L2-L1}}$ = −4.9 kcal mol^{-1} and $\Delta\Delta\Delta E_{\text{elstat,L4-L1}}$ = −3.7 kcal mol^{-1}). A similar pairwise comparison of the London dispersion effects shows that the difference in values between the system containing **L4** and the system containing **L1** ($\Delta\Delta\Delta E_{\text{disp,L4-L1}}$ = −4.3 kcal mol^{-1}) results mainly from the presence of the 16 methyl groups on **L4** that are not present in **L1**−**L3**.

Although the results above demonstrate that the peripheral methyl groups in **L4** cause the difference between the stabilizing dispersive interactions in the ground and transition states containing **L4** to be larger than this difference between those containing **L3** ($\Delta\Delta\Delta E_{\text{disp,L4-L3}}$

= −2.9 kcal mol^{-1}), we further probed the origin of this difference in dispersive interactions with ligands **L3** and **L4**. The methyl groups in **L4** could participate in stabilizing dispersive interactions with each other and with other groups in the complex, or they could cause the positions of the aryl groups and the structure of the core of the complexes of **L4** to be altered from those of **L1**−**L3** in a way that leads to a larger difference in dispersion interactions between the ground and transition states bearing **L4**. To distinguish between these two possibilities, we performed the same energy decomposition analysis of the ground and transition states with **L3** (lacking the peripheral methyl groups), but placing the atoms in the same positions as those in the lowest-energy geometry of **L4**. The results of this analysis are included in the Supplementary Information and show that the differences in dispersion interactions between the ground and transition states of the complexes containing **L4** and **L3** in the same geometry (the minimum-energy geometry of **L4**, $\Delta\Delta\Delta E_{\text{disp,L4-L3 in L4 geometry}}$ = −2.9 kcal mol^{-1}; Supplementary Table 12) are similar to those of the ground and transition states containing **L4** and **L3** in their respective minimum-energy geometries. In other words, the stabilizing dispersion interactions in the complexes of **L4** are due to direct interactions with the methyl groups, not to changes in the ligand geometry imparted by the methyl groups in **L4**. Finally, a graphical plot of the non-covalent interactions[51,52] present in $^{L4}\mathbf{TS}_{RE}$ (Supplementary Fig. 18) corroborates the presence of significant stabilizing interactions involving the methyl groups.

Conclusion

In this work the first highly anti-Markovnikov hydroarylation of unactivated alkenes with unactivated arenes has been accomplished, and many of the reactions occurred in good yields. Even internal alkenes reacted to give *n*-alkylarene products. The unparalleled selectivity and activity of this reaction was enabled by a nickel catalyst containing an extremely large N-heterocyclic carbene ligand that undergoes C–H activation by a mechanism that involves the formation of a linear alkyl–metal complex that undergoes reductive elimination to form the new carbon–carbon bond in the alkylarene product with rates that are enhanced by intramolecular non-covalent interactions. The results of our computational studies imply that the conventional view of how steric bulk favours reductive elimination does not apply to this system. Instead of accelerating the reductive elimination by steric repulsion, the multiple aryl groups in ligand **L4** of the most active catalyst lead to favourable electrostatic interactions, and the large number of methyl groups in **L4** leads to favourable London dispersion interactions and lower distortion energy. We anticipate that this reactivity and the analysis of its origins should aid the development of new methods for the functionalization of alkenes with additional strong, unactivated C–H or X–H bonds catalysed by complexes of nickel ligated by N-heterocyclic carbenes as well as by complexes of metals other than nickel with appropriate properties of the ancillary ligands.

Supplementary Material

Refer to Web version on PubMed Central for supplementary material.

Acknowledgements

We thank S. Arlow, C. Karmel and J. Wang for helpful discussions. We thank Y. Schramm for preliminary experiments. We acknowledge N. Settineri for X-ray crystallographic analysis. We thank M. Head-Gordon and M. Loipersberger for discussions on EDA calculations. This work was supported by the Director, Office of Science, of the U.S. Department of Energy under contract no. DE-AC02- 05CH11231, by the National Science Foundation (graduate research fellowship to N.I.S.) and by the Japan Society for the Promotion of Science (JSPS KAKENHI Grant Number JP15H05799). X-ray diffraction data were collected using an instrument funded by the NIH (S10-RR027172). Computations were performed on a computation cluster funded by the NIH (S10-OD023532). NMR spectroscopy was performed in the College of Chemistry's NMR facility funded in part by the NIH (S10-OD024998).

Data availability

Crystallographic data for the structures reported in this article have been deposited at the Cambridge Crystallographic Data Centre, under deposition numbers 1901576 ([**L4**–Ni(η^6-C_6H_6)]), 1901577 (**26**) and 1901578 (**25**). Copies of the data can be obtained free of charge via https://www.ccdc.cam.ac.uk/structures/. All other data supporting the findings of this study are available within the Article and its Supplementary Information, or from the corresponding author upon reasonable request.

References

1. Kocal JA, Vora BV & Imai T Production of linear alkylbenzenes. Appl. Catal. A 221, 295–301 (2001).
2. Linear Alkyl Benzene Market Size, Share & Trends Analysis Report By Application (Heavy Duty Laundry, Laundry Powders, Washing Liquids, Industrial Cleaners, Household Cleaners), And Segment Forecasts, 2012–2020 (Grand View Research, 2017).
3. Röper M, Gehrer E, Narbeshuber T & Siegel W Acylation and alkylation in Ullmann's Encyclopedia of Industrial Chemistry (Wiley-VCH, 2000).
4. de Almeida JLG, Dufaux M, Taarit YB & Naccache C Linear alkylbenzene. J. Am. Oil Chem. Soc 71, 675–694 (1994).
5. Ishiwatari R, Takada H, Yun S-J & Matsumoto E Alkylbenzene pollution of Tokyo Bay sediments. Nature 301, 599–600 (1983).
6. Macías-Zamora JV & Ramírez-Alvarez N Tracing sewage pollution using linear alkylbenzenes (LABs) in surface sediments at the south end of the Southern California Bight. Environ. Pollut 130, 229–238 (2004). [PubMed: 15158036]
7. Murai S et al. Efficient catalytic addition of aromatic carbon-hydrogen bonds to olefins. Nature 366, 529–531 (1993).
8. Jun C-H, Hong J-B, Kim Y-H & Chung K-Y The catalytic alkylation of aromatic imines by Wilkinson's complex: the domino reaction of hydroacylation and *ortho*-alkylation. Angew. Chem. Int. Ed 39, 3440–3442 (2000).
9. Gao K & Yoshikai N Cobalt–phenanthroline catalysts for the *ortho* alkylation of aromatic imines under mild reaction conditions. Angew. Chem. Int. Ed 50, 6888–6892 (2011).
10. Schinkel M, Marek I & Ackermann L Carboxylate-assisted ruthenium(II)-catalyzed hydroarylations of unactivated alkenes through C–H cleavage. Angew. Chem. Int. Ed 52, 3977–3980 (2013).
11. Matsumoto T, Taube DJ, Periana RA, Taube H & Yoshida H Anti-Markovnikov olefin arylation catalyzed by an iridium complex. J. Am. Chem. Soc 122, 7414–7415 (2000).
12. Periana RA, Liu XY & Bhalla G Novel bis-acac-O,O–Ir(III) catalyst for anti-Markovnikov, hydroarylation of olefins operates by arene CH activation. Chem. Commun 24, 3000–3001 (2002).
13. Oxgaard J, Muller RP, Goddard WA & Periana RA Mechanism of homogeneous Ir(III) catalyzed regioselective arylation of olefins. J. Am. Chem. Soc 126, 352–363 (2004). [PubMed: 14709102]

14. Bhalla G, Liu XY, Oxgaard J, Goddard WA & Periana RA Synthesis, structure, and reactivity of O-donor Ir(III) complexes: C–H activation studies with benzene. J. Am. Chem. Soc 127, 11372–11389 (2005). [PubMed: 16089467]
15. Bhalla G, Oxgaard J, Goddard WA & Periana RA Anti-Markovnikov hydroarylation of unactivated olefins catalyzed by a bis-tropolonato iridium(III) organometallic complex. Organometallics 24, 3229–3232 (2005).
16. Lail M, Arrowood BN & Gunnoe TB Addition of arenes to ethylene and propene catalyzed by ruthenium. J. Am. Chem. Soc 125, 7506–7507 (2003). [PubMed: 12812477]
17. Lail M et al. Experimental and computational studies of ruthenium(II)-catalyzed addition of arene C−H bonds to olefins. Organometallics 23, 5007–5020 (2004).
18. McKeown BA, Prince BM, Ramiro Z, Gunnoe TB & Cundari TR Pt^{II}-catalyzed hydrophenylation of α-olefins: variation of linear/branched products as a function of ligand donor ability. ACS Catal. 4, 1607–1615 (2014).
19. Luedtke AT & Goldberg KI Intermolecular hydroarylation of unactivated olefins catalyzed by homogeneous platinum complexes. Angew. Chem. Int. Ed 47, 7694–7696 (2008).
20. Clement ML, Grice KA, Luedtke AT, Kaminsky W & Goldberg KI Platinum(II) olefin hydroarylation catalysts: tuning selectivity for the anti-Markovnikov product. Chem. Eur. J 20, 17287–17291 (2014). [PubMed: 25377546]
21. Webster-Gardiner MS et al. Catalytic synthesis of “super” linear alkenyl arenes using an easily prepared Rh(I) catalyst. J. Am. Chem. Soc 139, 5474–5480 (2017). [PubMed: 28383890]
22. Chen J et al. Catalytic synthesis of superlinear alkenyl arenes using a Rh(I) catalyst supported by a “capping arene” ligand: access to aerobic catalysis. J. Am. Chem. Soc 140, 17007–17018 (2018). [PubMed: 30495938]
23. Oxgaard J & Goddard WA Mechanism of Ru(II)-catalyzed olefin insertion and C−H activation from quantum chemical studies. J. Am. Chem. Soc 126, 442–443 (2004). [PubMed: 14719922]
24. Oxgaard J, Periana RA & Goddard WA Mechanistic analysis of hydroarylation catalysts. J. Am. Chem. Soc 126, 11658–11665 (2004). [PubMed: 15366913]
25. Suslick BA, Liberman-Martin AL, Wambach TC & Tilley TD Olefin hydroarylation catalyzed by (pyridyl-indolate)Pt(II) complexes: catalytic efficiencies and mechanistic aspects. ACS Catal. 7, 4313–4322 (2017).
26. Mann G, Shelby Q, Roy AH & Hartwig JF Electronic and steric effects on the reductive elimination of diaryl ethers from palladium(II). Organometallics 22, 2775–2789 (2003).
27. Foley NA et al. Comparative reactivity of TpRu(L)(NCMe)Ph (L = CO or PMe_3): impact of ancillary ligand L on activation of carbon–hydrogen bonds including catalytic hydroarylation and hydrovinylation/oligomerization of ethylene. J. Am. Chem. Soc 129, 6765–6781 (2007). [PubMed: 17488072]
28. Foley NA, Ke Z, Gunnoe TB, Cundari TR & Petersen JL Aromatic C−H activation and catalytic hydrophenylation of ethylene by TpRu{$P(OCH_2)_3CEt$}(NCMe)Ph. Organometallics 27, 3007–3017 (2008).
29. Foley NA, Lee JP, Ke Z, Gunnoe TB & Cundari TR Ru(II) catalysts supported by hydridotris(pyrazolyl)borate for the hydroarylation of olefins: reaction scope, mechanistic studies, and guides for the development of improved catalysts. Acc. Chem. Res 42, 585–597 (2009). [PubMed: 19296659]
30. Joslin EE et al. Catalytic hydroarylation of ethylene using TpRu(L)(NCMe) Ph (L = 2,6,7-trioxa-1-phosphabicyclo[2,2,1]heptane): comparison to TpRu(L′)(NCMe)Ph systems (L′ = CO, PMe_3, $P(pyr)_3$, or $P(OCH_2)_3CEt$). Organometallics 31, 6851–6860 (2012).
31. Burgess SA et al. Hydrophenylation of ethylene using a cationic Ru(ii) catalyst: comparison to a neutral Ru(ii) catalyst. Chem. Sci 5, 4355–4366 (2014).
32. Malinoski JM & Brookhart M Polymerization and oligomerization of ethylene by cationic nickel(II) and palladium(II) complexes containing bidentate phenacyldiarylphosphine ligands. Organometallics 22, 5324–5335 (2003).
33. Bair JS et al. Linear-selective hydroarylation of unactivated terminal and internal olefins with trifluoromethyl-substituted arenes. J. Am. Chem. Soc 136, 13098–13101 (2014). [PubMed: 25171744]

34. Schramm Y, Takeuchi M, Semba K, Nakao Y & Hartwig JF Anti-Markovnikov hydroheteroarylation of unactivated alkenes with indoles, pyrroles, benzofurans, and furans catalyzed by a nickel–N-heterocyclic carbene cystem. J. Am. Chem. Soc 137, 12215–12218 (2015). [PubMed: 26334367]
35. Guihaumé J, Halbert S, Eisenstein O & Perutz RN Hydrofluoroarylation of alkynes with Ni catalysts. C−H activation via ligand-to-ligand hydrogen transfer, an alternative to oxidative addition. Organometallics 31, 1300–1314 (2012).
36. Hoshimoto Y, Hayashi Y, Suzuki H, Ohashi M & Ogoshi S One-pot, single-step, and gram-scale synthesis of nononuclear [(η^6-arene)Ni(N-heterocyclic carbene)] complexes: useful precursors of the Ni^0–NHC unit. Organometallics 33, 1276–1282 (2014).
37. Berthon-Gelloz G et al. IPr* an easily accessible highly hindered N-heterocyclic carbene. Dalton Trans. 39, 1444–1446 (2010). [PubMed: 20104298]
38. Meiries S, Speck K, Cordes DB, Slawin AMZ & Nolan SP [Pd(IPr^{*OMe})(acac)Cl]: tuning the *N*-heterocyclic carbene in catalytic C−N bond formation. Organometallics 32, 330–339 (2013).
39. Okumura S et al. *para*-Selective alkylation of benzamides and aromatic ketones by cooperative nickel/aluminum catalysis. J. Am. Chem. Soc 138, 14699–14704 (2016). [PubMed: 27759372]
40. Horn PR, Mao Y & Head-Gordon M Probing non-covalent interactions with a second generation energy decomposition analysis using absolutely localized molecular orbitals. Phys. Chem. Chem. Phys 18, 23067–23079 (2016). [PubMed: 27492057]
41. Saper NI & Hartwig JF Mechanistic investigations of the hydrogenolysis of diaryl ethers catalyzed by nickel complexes of N-heterocyclic carbene ligands. J. Am. Chem. Soc 139, 17667–17676 (2017). [PubMed: 29116776]
42. Clavier H & Nolan SP Percent buried volume for phosphine and N-heterocyclic carbene ligands: steric properties in organometallic chemistry. Chem. Commun 46, 841–861 (2010).
43. Hillier AC et al. A combined experimental and theoretical study examining the binding of N-heterocyclic carbenes (NHC) to the Cp*RuCl (Cp* = η^5-C_5Me_5) moiety: insight into stereoelectronic differences between unsaturated and saturated NHC ligands. Organometallics 22, 4322–4326 (2003).
44. Falivene L et al. SambVca 2. A web tool for analyzing catalytic pockets with topographic steric maps. Organometallics 35, 2286–2293 (2016).
45. Dorta R et al. Steric and electronic properties of *N*-heterocyclic carbenes (NHC): a detailed study on their interaction with $Ni(CO)_4$. J. Am. Chem. Soc 127, 2485–2496 (2005). [PubMed: 15725003]
46. Matsumoto T, Periana RA, Taube DJ & Yoshida H Regioselective hydrophenylation of olefins catalyzed by an Ir(III) complex. J. Mol. Catal. A 180, 1–18 (2002).
47. Simmons EM & Hartwig JF On the interpretation of deuterium kinetic isotope effects in C−H bond functionalizations by transition-metal complexes. Angew. Chem. Int. Ed 51, 3066–3072 (2012).
48. Tang S, Eisenstein O, Nakao Y & Sakaki S Aromatic C–H σ-bond activation by Ni^0, Pd^0, and Pt^0 alkene complexes: concerted oxidative addition to metal vs ligand-to-ligand H transfer mechanism. Organometallics 36, 2761–2771 (2017).
49. Bickelhaupt FM & Houk KN Analyzing reaction rates with the distortion/interaction-activation strain model. Angew. Chem. Int. Ed 56, 10070–10086 (2017).
50. Hartwig JF in Organotransition Metal Chemistry: From Bonding to Catalysis Ch. 8 (Univ. Science Books, 2010).
51. Johnson ER et al. Revealing noncovalent interactions. J. Am. Chem. Soc 132, 6498–6506 (2010). [PubMed: 20394428]
52. Contreras-García J et al. NCIPLOT: a program for plotting noncovalent interaction regions. J. Chem. Theory Comput 7, 625–632 (2011). [PubMed: 21516178]

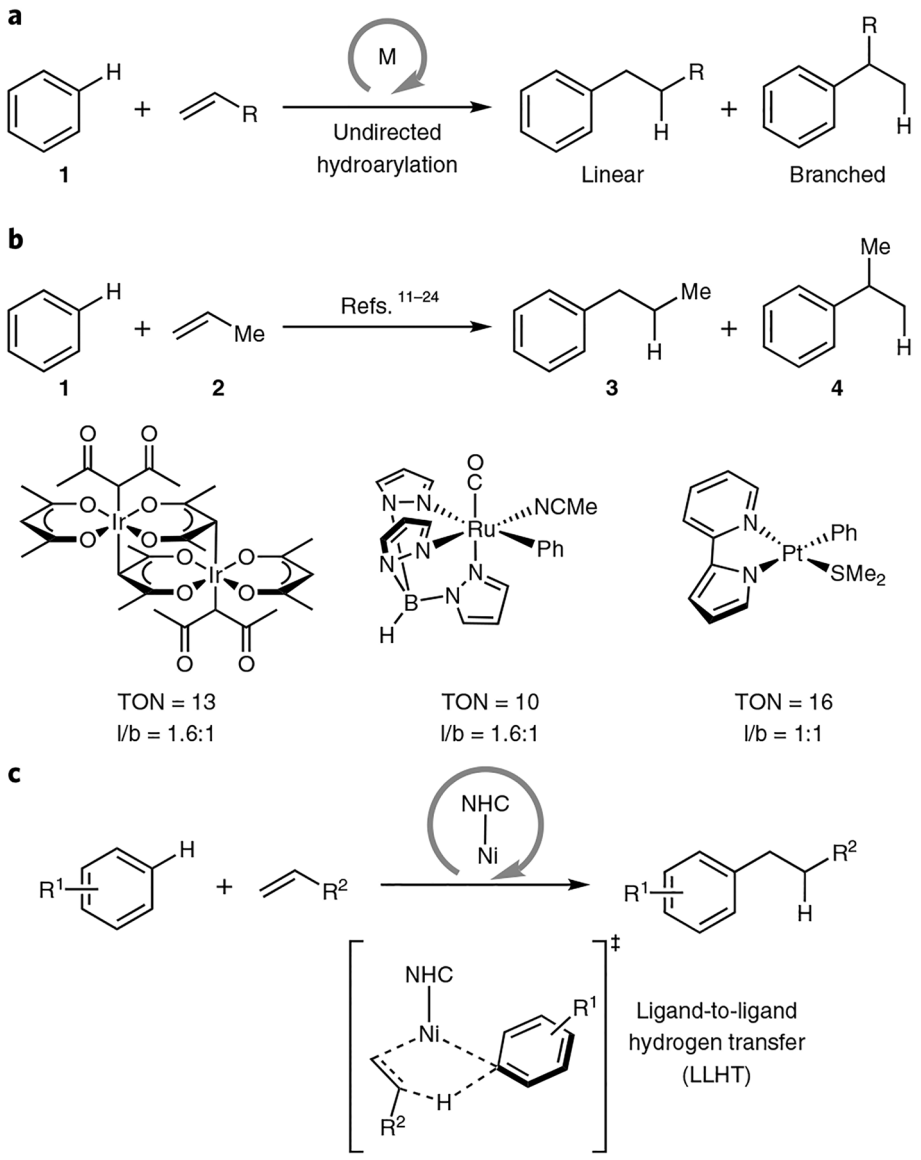

Fig. 1 |. Transition metal-catalysed hydroarylation of unactivated alkenes with unactivated arenes.

a, Linear and branched isomeric products formed by undirected transition-metal-catalysed hydroarylation. **b**, State-of-the-art catalytic systems for the hydroarylation reaction of benzene with propylene with the turnover numbers (TONs) and linear/branched (l/b) ratios indicated. **c**, The linear-selective hydroarylation reaction described in this report.

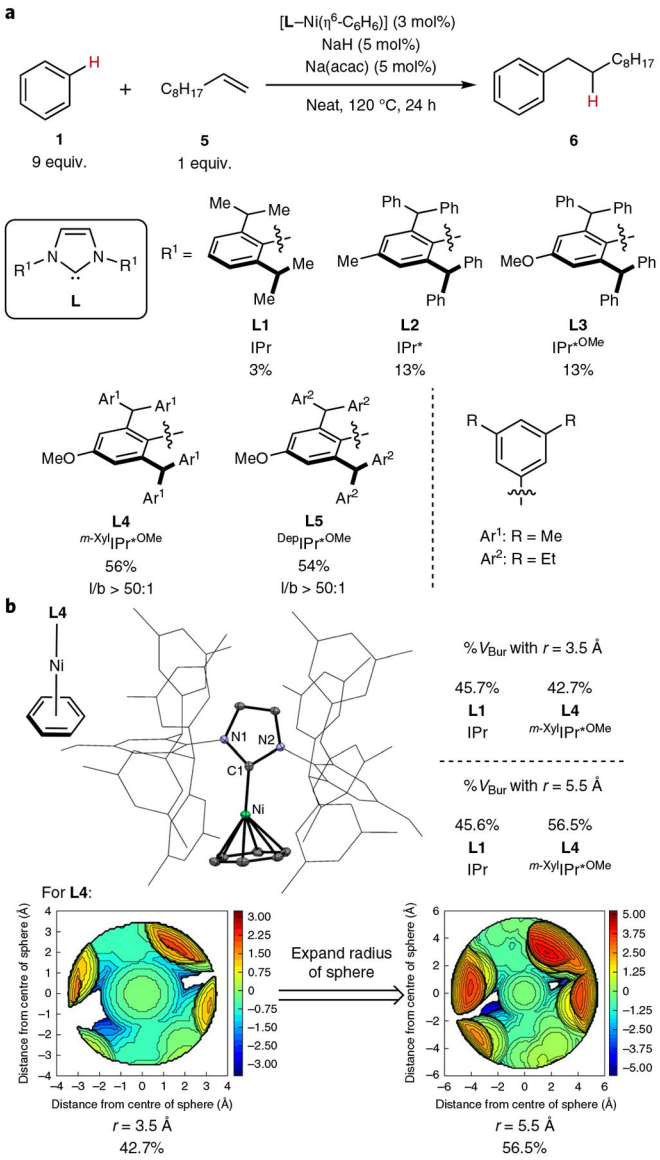

Fig. 2 |. Reaction development and characterization of [L4–Ni(η^6-C_6H_6)].

a, Identifying NhC ligands to achieve hydroarylation. Yields and linear/branched (l/b) ratios were determined by GC or NMr spectroscopic analysis of the crude reaction mixture. **b**, OrTEP diagram of [**L4**–Ni(η^6-C_6h_6)] (thermal ellipsoids are shown at the 50% probability level), calculated % V_{Bur} values and steric map. An expanded radius of 5.5 Å for the % V_{Bur} calculation was necessary to account for the remote steric environment of **L4**. The origins of the steric maps depicted are centred 2.0 Å away from the carbene carbon atoms with the +*z* axis defined by the carbene carbons and the midpoints between the two backbone carbons, and the (*x*,*z*) planes are defined by the two backbone carbons and the carbene carbon atoms. Additional details of the calculations of the % V_{Bur} values can be found in the Supplementary Information. For clarity, all hydrogen atoms have been omitted from the OrTEP diagram, and NhC sidearms are represented in wire format.

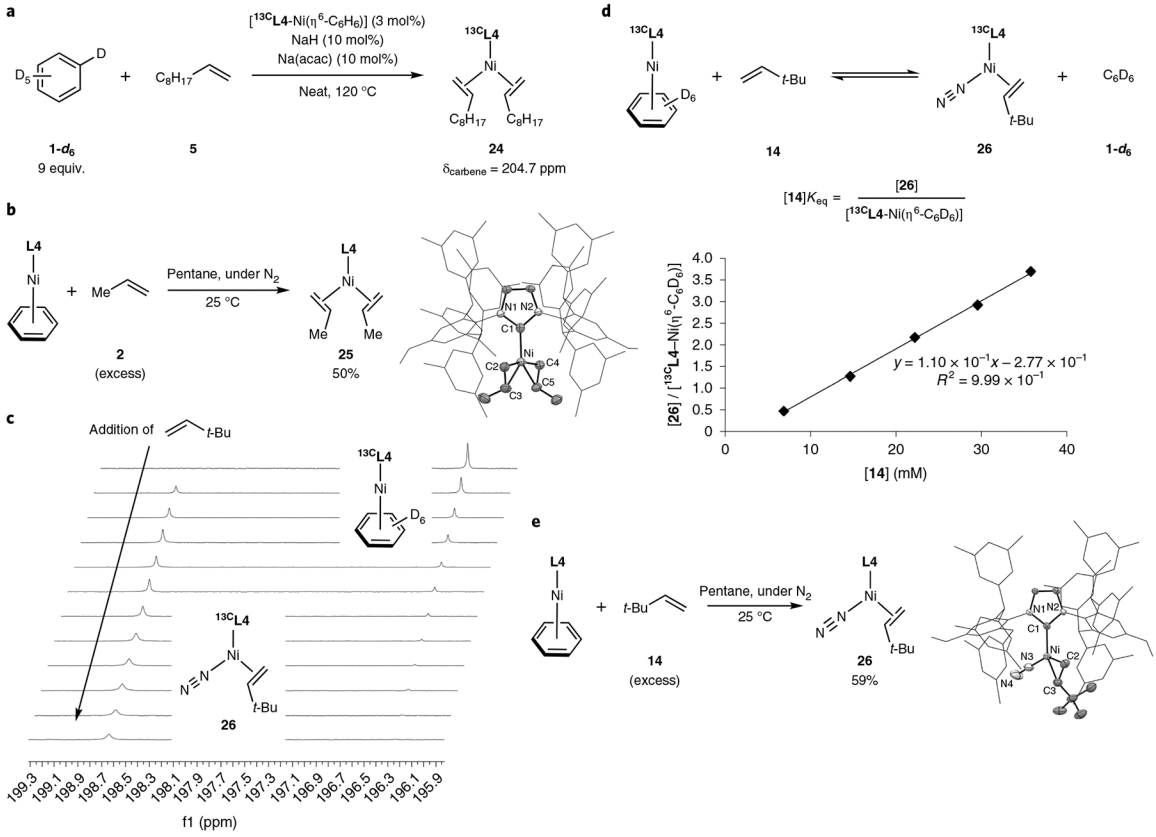

Fig. 3 |. Observation and isolation of catalyst resting states.

a, Observation of the catalyst resting state in the hydroarylation reaction of **1-*d*$_6$** with unhindered alkene **5** by ^{13}C NMR spectroscopy. The resting state with unhindered alkene **5** was found to be complex **24. b**, Preparation of bis-olefin complex **25** and the ORTEP diagram of the X-ray diffraction structure of **25** (thermal ellipsoids are shown at the 50% probability level). **c**, The equilibrium between **[^{13C}L4**–Ni(η^6-C$_6$H$_6$)] and the mono-olefin complex **26** was monitored by ^{13}C NMR spectroscopy. The spectra resulting from the addition of **14** (0–60 equiv.) to a solution of [**^{13C}L4**–Ni(η^6-C$_6$H$_6$)] in C$_6$D$_6$ are shown. **d**, Expression for the equilibrium between arene- and alkene-bound **^{13C}L4**–Ni complexes and a plot of the ratio of nickel complexes with respect to [**14**]. We estimate the error in the integral ratios to be <5% based on the signal-to-noise ratio of the ^{13}C NMR spectra. **e**, Preparation of mono-olefin complex **26** and ORTEP diagram of the the X-ray diffraction structure of **26** (thermal ellipsoids are shown at the 50% probability level). For clarity, all hydrogen atoms have been omitted from the ORTEP diagrams, and NHC sidearms are represented in wire format.

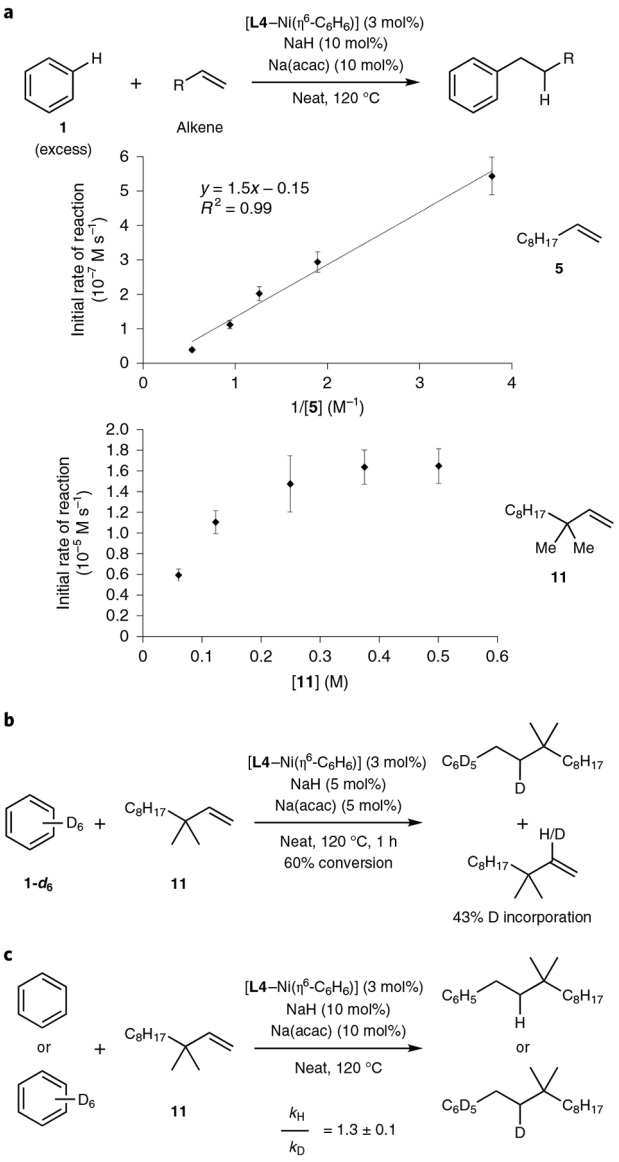

Fig. 4 |. Mechanistic experiments.

a, Dependence of the initial rate of the hydroarylation on alkene concentration for unhindered alkene **5** (top) or hindered alkene **11** (bottom). Error bars indicate a ±10% error in the initial rate. **b**, Deuterium incorporation was observed at the 2-alkenyl position of unreacted alkene **11** in the hydroarylation of **11** with **1-*d*$_6$**. **c**, A KIE experiment for the hydroarylation of alkene **11** was conducted in separate vessels, and the KIE was found to be 1.3 ± 0.1. This result indicates that hydrogen atom transfer is reversible.

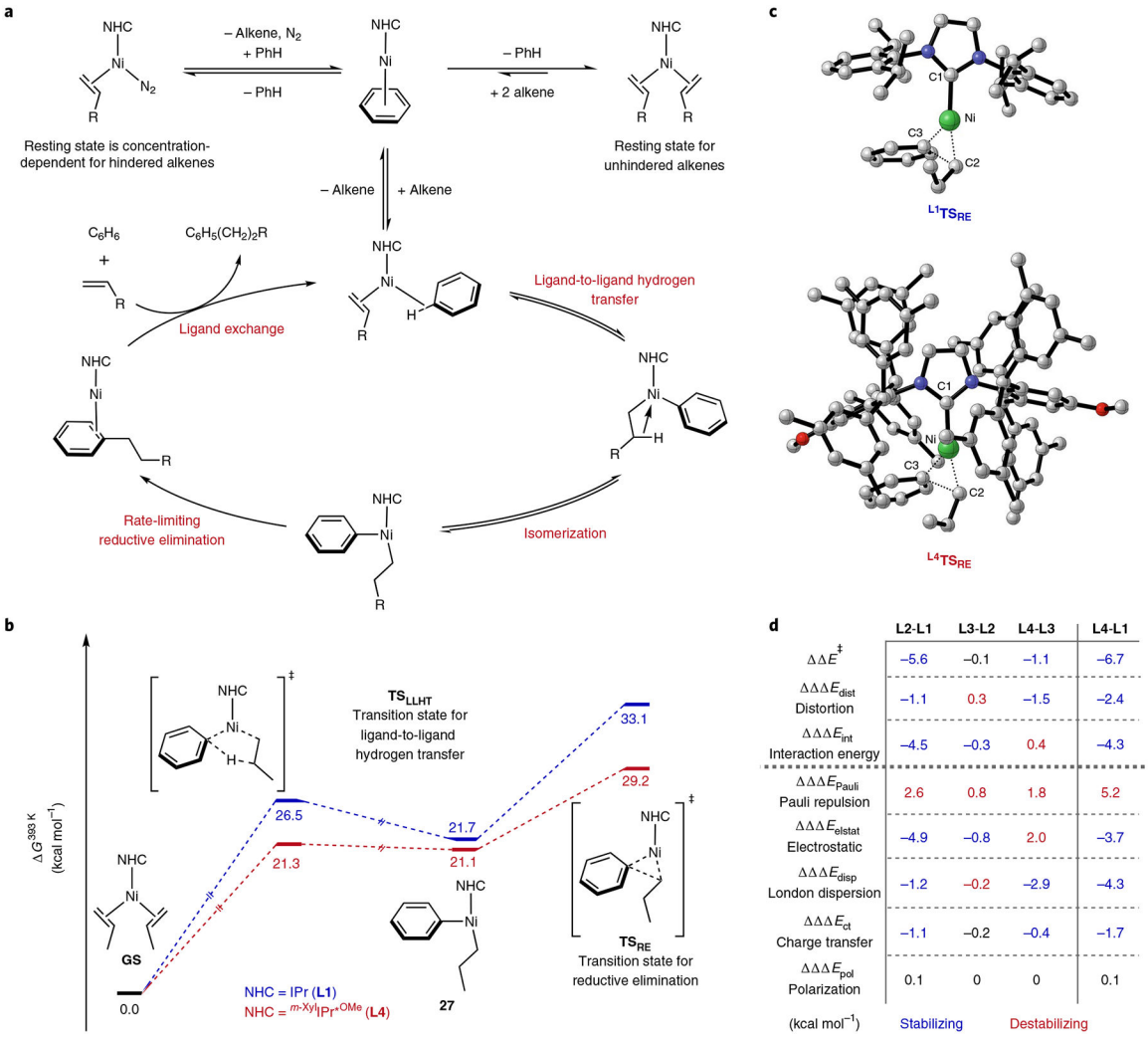

Fig. 5 |. Computational investigations.

a, Proposed mechanism for the nickel-catalysed hydroarylation of unactivated alkenes supported by mechanistic experiments and computations. **b**, Computed energetics for the hydroarylation reaction with catalysts containing **L1** and **L4**. **c**, DFT-optimized geometries of $\mathbf{TS}_{RE}$. **d**, Energy decomposition analysis for the changes between the ground state and transition state for reductive elimination as a function of the carbene ligand. ΔE_{dist} is the difference in energy between the most stable form of the free carbene ligand and free nickel fragment and the energy of the two components in their geometries of the complex, $\Delta\Delta E_{dist}$ is the difference in distortion energies between the ground state and transition state and $\Delta\Delta\Delta E_{dist}$ is the difference in $\Delta\Delta E_{dist}$ for the pairs of ligands. ΔE_{int} is the interaction energy of the two fragments in their distorted geometries and is decomposed as the sum of ΔE_{Pauli}, ΔE_{elstat}, ΔE_{disp}, ΔE_{ct} and ΔE_{pol}. In a similar manner, $\Delta\Delta E$ values are the difference in energies between the **GS** and the **TS**, and $\Delta\Delta\Delta E$ values are the difference in the component $\Delta\Delta E$ for pairs of ligands.

Table 1 |

Scope of the hydroarylation reaction

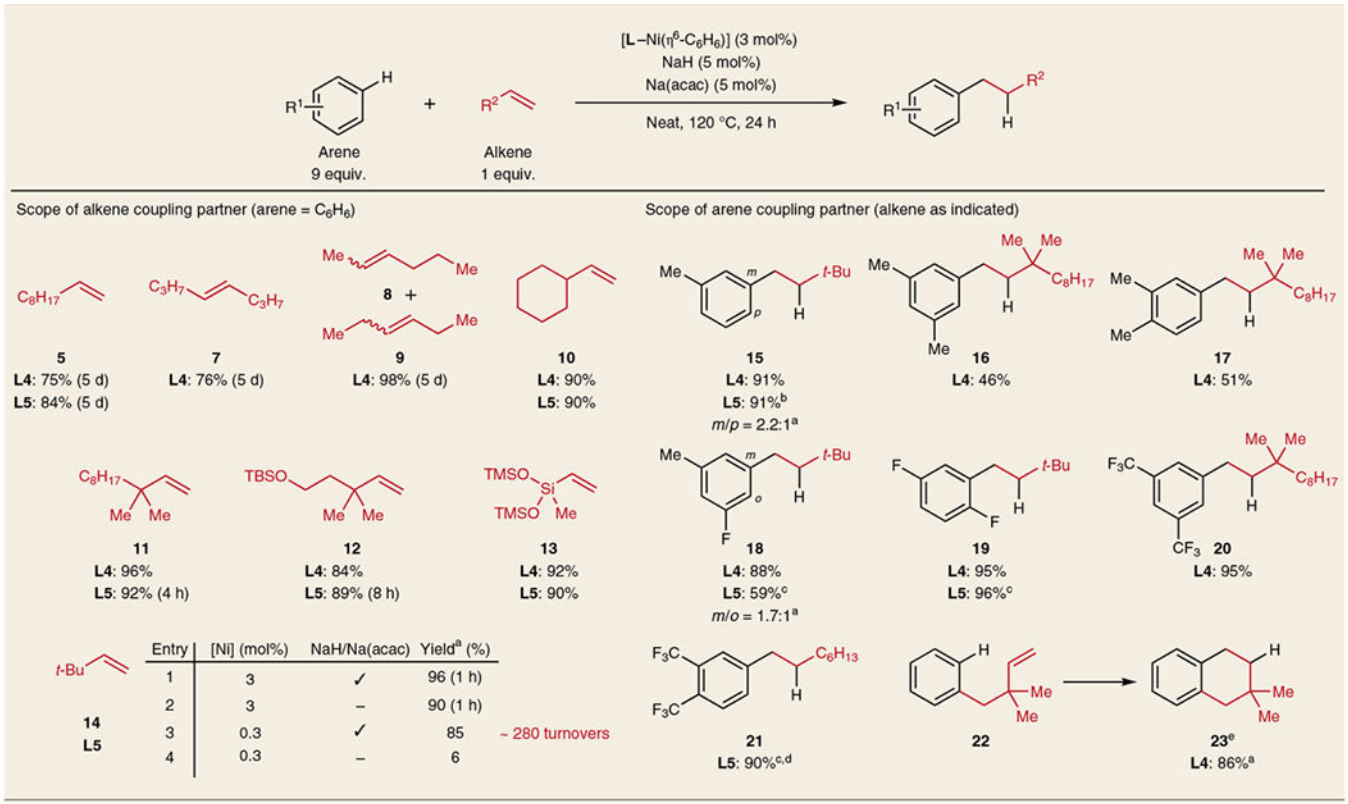

[a]Determined by GC or NMr spectroscopic analysis of the crude reaction mixture.

[b]18 equiv. of arene were added.

[c]3 equiv. of arene were added.

[d]Nah and Na(acac) were excluded.

[e]Mesitylene was added as the reaction solvent.